Fragmentation of a circular disc by impact on a frictionless plate

2005 J. Phys.: Condens. Matter 17 S2439

(http://iopscience.iop.org/0953-8984/17/24/005)

INSTITUTE OF PHYSICS PUBLISHING JOURNAL OF PHYSICS: CONDENSED MATTER

J. Phys.: Condens. Matter **17** (2005) S2439–S2456 doi:10.1088/0953-8984/17/24/005

Fragmentation of a circular disc by impact on a frictionless plate

Bhupalendra Behera[1,2], **Ferenc Kun**[3], **Sean McNamara**[1] **and Hans J Herrmann**[1]

[1] Institut für Computeranwendungen (ICA1), Universität Stuttgart, 70569 Stuttgart, Germany
[2] Indian Institute of Technology, Department of Materials and Metallurgical Engineering, Kanpur, India
[3] Department of Theoretical Physics, University of Debrecen, H-4010 Debrecen, PO Box 5, Hungary

E-mail: feri@dtp.atomki.hu

Received 16 March 2005
Published 3 June 2005
Online at stacks.iop.org/JPhysCM/17/S2439

Abstract

The break-up of a two-dimensional circular disc by normal and oblique impact on a hard frictionless plate is investigated by molecular dynamics simulations. The disc is composed of numerous unbreakable randomly shaped convex polygons connected together by simple elastic beams that break when bent or stretched beyond a certain limit. It is found that for both normal and oblique impacts the crack patterns are the same and depend solely on the normal component of the impact velocity. Analysing the pattern of breakage, amount of damage, fragment masses and velocities, we show the existence of a critical velocity which separates two regimes of the impact process: below the critical point only a damage cone is formed at the impact site (*damage*), cleaving of the particle occurs at the critical point, while above the critical velocity the disc breaks into several pieces (*fragmentation*). In the limit of very high impact velocities the disc suffers complete disintegration (*shattering*) into many small fragments. In agreement with experimental results, fragment masses are found to follow the Gates–Gaudin–Schuhmann distribution (power law) with an exponent independent of the velocity and angle of impact. The velocity distribution of fragments exhibits an interesting anomalous scaling behaviour when changing the impact velocity and the size of the disc.

(Some figures in this article are in colour only in the electronic version)

1. Introduction

The strength and break-up of agglomerates composed of smaller sized primary particles is of particular importance for the storage and handling of materials in process industries such as pharmaceuticals, chemicals, fertilizers, detergent, and food industries. In industrial processes

agglomerates often collide with each other and with the hard walls of the equipment, resulting in a size reduction, which is desired or not depending on the type of the process. The strength of agglomerates has to be characterized for the design of operating conditions in industrial processes such as milling, tabletting, mixing, and transport in pneumatic conveying. Another important class of agglomerates are the so-called particle compounds, which are the combination of various sized particles embedded in a cementous matrix. The different types of engineering agglomerates and building materials like concretes are some examples of particle compounds. It is of high industrial importance to recycle these particle compounds in order to use the valuable aggregates. The design and optimization of the liberation process of aggregates from the matrix material requires a detailed knowledge of the strength and break-up of compounds.

For the understanding of the strength and break-up process, the study of simple systems like spherical particles is essential. During the last decades several experimental and theoretical studies have been performed to understand the break-up of spherical bodies arising due to impact. The crack pattern of sand–cement spheres by a free fall impact was studied in [1], which reports observations of meridian cracks, that divide the sphere into two nearly equal parts, and oblique cracks, which are straight like median cracks, but cut the sphere into two unequal pieces. The fracture of glass and plaster spheres by free fall impact and double impact (dynamic loading between two hard plates) have been carried out recently [2, 3]. It was found that at the lowest impact velocities Hertzian cone cracks (formed from a surface ring crack) are developed, whereas at high velocities oblique cracks propagate before meridian cracks form [4]. This finding differs from the experimental results of [1], where it was found that with increasing impact energy the number of meridian planes increases and oblique cracks start to develop.

Due to the high speed and violent nature of the break-up process, observations are usually restricted to the final state of impact experiments, where information has to be extracted from the remaining pieces of the body. Hence, computer simulation of models of agglomerate break-up is an indispensable tool in this field. Simulations of realistic models provide a deeper insight into the break-up process and can even complement the experimental findings, directly supporting the design of industrial processing of these materials. Analytic approaches have limited capabilities in this field since they cannot capture the disordered microstructure of the material.

The finite element approach and discrete element modelling have been successfully applied to describe the stress field, crack propagation, and fragment formation in impacting spherical particles [7, 8, 27, 31, 32, 34, 38, 40, 41]. Recent simulations of ball impact revealed two types of crack patterns: oblique cracks radiating from the impact point, and secondary cracks perpendicular to the oblique ones. In the framework of the discrete element method it was clarified that depending on the impact velocity the result of the break-up process can be localized damage around the contact zone, fragmentation, or shattering. The evolution of several characteristic quantities of the break-up process when increasing the impact velocity were monitored and analysed in normal and oblique impact [7, 8, 27, 31, 34].

From a more general point of view, the break-up of agglomerates presents an important class of fragmentation phenomena which is ubiquitous in everyday life and concerns a wide range of phenomena in science and technology. In general, when an object is subjected to shock or stress it will break up into smaller pieces. The length scales involved in this process range from the collisional evolution of asteroids [6] to the degradation of materials comprised of small agglomerates [7, 8] employed in the process industries as summarized above. There are also many geological examples associated with the use of explosives for mining and oil shale industry, coal heaps, etc. A wide variety of experiments [13–15, 22–24, 26, 28, 30, 37]

and simulations [7–12, 16–21, 27, 38] revealed that the fragment mass distribution is a power law except for very large fragment sizes. The exponents in the power law region were found experimentally to be between 1.35 and 2.6 depending on the effective dimensionality of the system [1, 6, 24, 25]. Recent studies revealed that power law distributions arise in fragmentation phenomena due to an underlying phase transition [10, 21, 26]. However, most of the data reported in the literature are concerned with the general behaviour of fragmentation processes. There is much less literature where the propagation and orientation of cracks are discussed.

In the present paper we study the normal and oblique impact of a circular brittle particle on a hard frictionless plate, varying the impact velocity and impact angle in a broad range. The particle is composed of numerous unbreakable, undeformable, randomly shaped polygons which are bonded together by elastic beams. The bonds between the polygons can be broken according to a physical breaking rule, which takes into account the stretching and bending of the connections. Based on simulations of the model, we performed a detailed study of the failure evolution at different impact velocities and of the nature of the crack propagation during the fragmentation process, and compared the results with experiments [1, 2, 4, 22, 24]. In the analysis of the simulation data, we profit from recent theoretical results of general studies of fragmentation processes. We observed that for both normal and oblique impacts the crack patterns are the same and depend solely on the normal component of the impact velocity. Studying the crack patterns, amount of damage, fragment masses, and velocities, we provide a quantitative foundation of the concept of damage, fragmentation, and shattering in ball impact, which was introduced recently on a more qualitative basis [7]. We show the existence of a critical impact velocity v_c which distinguishes two regimes of the impact process, i.e. below the critical velocity damage mainly occurs in a conical region around the impact site with a large residue; however, above v_c an ensemble of oblique cracks develops and the disc breaks up into pieces. In agreement with experimental results, fragment masses are found to follow the Gates–Gaudin–Schuhmann distribution (power law) [35] with an exponent independent of the velocity and angle of impact. The velocity distribution of fragments exhibits an interesting anomalous scaling behaviour when changing the impact velocity and the size of the disc.

An important application of our results, besides the ones mentioned at the beginning, is to the optimization and control of tumbling mill performance. These questions are of utmost practical importance as they have a tremendous influence on power draft, wear of the balls and liners and breakage characteristics of the grinding materials. During the cataracting motion where the charge material inside a mill follows a parabolic path [5], most of the materials are ground as hard balls fall back onto them. There is particular interest in the net energy required to achieve a certain size reduction and the energy distribution of the fragments during the grinding process. The efficiency of the mills could be controlled if the breakage characteristics of the grinding materials were better understood. Our current work can provide some valuable information for the modernization of the mill design.

2. Model

In order to study fragmentation of granular solids, we performed molecular dynamic (MD) simulations in two dimensions. To better capture the complex structure of a real solid, we used randomly generated convex polygons that interact with each other elastically. The model consists of three major parts, namely, the construction of a Voronoi cellular structure, the introduction of the elastic behaviour, and finally the breaking of the solid. This section gives a detailed overview of these three steps.

In order to take into account the complex structure of the granular solid, we use randomly generated convex polygons, i.e. we divide the solid into grains by a Voronoi cellular structure.

The Voronoi construction is a random tessellation of the plane into convex polygons. This is obtained by putting a random set of points onto the plane and then assigning to each point that part of the plane which is nearer to it than to any other point. One advantage of the Voronoi tessellation is that the number of neighbours of each polygon is limited, which makes the computer code faster and allows us to simulate larger systems. In our case, the initial configuration of the polygons was constructed using a vectorizable random lattice, which is a Voronoi construction with slightly reduced disorder [36]. First the Voronoi tessellation of a square is performed, and then a circular disc with smooth surface is cut out.

In the model the polygons are rigid bodies. They are neither breakable nor deformable, but they can overlap when pressed against each other. This overlap represents local deformations of the grains. Usually the overlapping polygons have two intersection points which define the contact line. In order to simulate the elastic contact force, we introduce a repulsive force between touching polygons. This force is proportional to the overlapping area A divided by a characteristic length L_c ($\frac{1}{L_c} = \frac{1}{2}[\frac{1}{r_i} + \frac{1}{r_j}]$, where r_i and r_j are the radii of circles of the same area as the polygons). The direction of the elastic or normal force is perpendicular to the contact line of the polygons. The complete form of the normal force contains an elastic and damping contribution, whereas the tangential component is responsible for the friction.

Again, to bond the particles together it is necessary to introduce a cohesive force between neighbouring polygons. For this purpose we introduce beams. The centres of mass of neighbouring polygons are joined together with elastic beams that exert an attractive, restoring force but can break in order to model the fragmentation of the solid. Because of the randomness contained in the Voronoi tessellation, the lattice of beams is also random. The length, the cross-section and the moment of inertia of each beam are determined by the initial configuration of the polygons. The Young moduli of the beams and of the particles are considered to be independent of each other. The beams break according to a physical breaking rule, which takes into account the stretching and bending of the connection. The surface of the grains where beams are broken represents cracks. The energy stored in the broken beams represents the energy needed to create these new crack surfaces inside the solid.

In order to simulate the break-up of the disc due to impact with a hard plate, a repulsive force is introduced between the plate and those polygons of the disc which have overlap with the plate. This repulsive force is proportional to the overlap area, similar to the polygon–polygon contacts but with a higher stiffness value. The contact force of the disc and the plate has vertical direction; a tangential component like friction is excluded in the present study.

The time evolution of the system is obtained by numerically solving Newton's equations of motion of the individual polygons (molecular dynamics). For the solution of the equations we use a gear predictor–corrector scheme of fifth order, which means that we have to keep track of the coordinates and all their derivatives up to fifth order. The breaking criterion of beams is evaluated in each iteration time step and those beams which fulfil the condition are removed from the calculations. The simulation stops after no beams break during a certain number of time steps. Previously this model has been applied to study fragmentation of solids in various experimental situations [9–12, 39]. For more details of the simulation technique see [9].

3. Crack pattern

In the present work we apply our model to explore the properties of the fragmentation process of a circular disc when dropped on a frictionless hard plate at different angles. The particle moves with a constant speed v_0 without the influence of gravity, which is obtained by supplying a constant velocity to all the polygons constituting the circular particle just before it touches

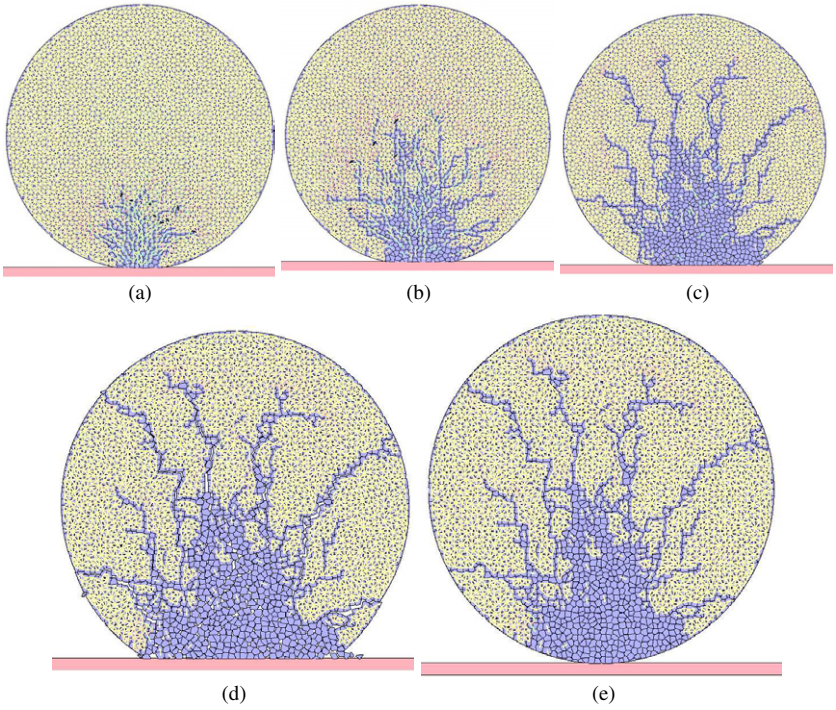

Figure 1. Snapshots of the fragmentation process in normal impact of a circular disc of radius 30 cm at 250 cm s^{-1}. (a) $t = 0.001\,50$ s, a high compressive wave generated at the impact point causes the primary breakage. (b) $t = 0.003\,00$ s, cracks start at the periphery of the conical region whose base is the contact line between the disc and the plate. (c) $t = 0.006\,00$ s, oblique cracks move outwards. (d) $t = 0.009\,96$ s, the oblique cracks reach at the outer surface. (e) The disc is reassembled at the end of the simulation to observe the final crack pattern.

the hard surface. The impact angle θ, defined as the angle of the vector of the impact velocity to the horizontal, was varied between 90° (normal impact) and 45° (oblique impact).

In order to understand the break-up process of discs, we investigated the crack pattern arising both in normal and oblique impacts. Figure 1 presents the time evolution of the crack pattern of normal impact obtained by the simulation of a circular disc of radius 30 cm at 250 cm s^{-1}. When the disc strikes against the hard plate, a highly compressive wave is generated at the impact point. Fracture starts from the region of the contact point and propagates through the disc. As the time passes, more and more bonds break at the impact region and the area of contact increases progressively. As a result of this primary breakage a cone shaped (triangle shaped in two dimensions) damage area is created whose base corresponds approximately to the area of contact of the specimen and the target (see figure 1(b)) and it is more distinct at the end of the fragmentation process (see figure 1(d)). When the cone is driven into the specimen a large number of cracks are generated starting from the region around the cone (see figure 1(b)). This indicates that a high stress concentration has developed around the conical damage region. Later on these cracks run together to form a few oblique cracks (see figure 1(c)) directed radially outward. As crack propagation is very energy dissipative, when these oblique cracks move outwards, the intensity of the compressive wave gradually decreases and hence larger fragments appear opposite the impact point.

To demonstrate the effect of the impact velocity on the break-up process, in figure 2 final states of the process are shown obtained at different impact velocities, with the fragments

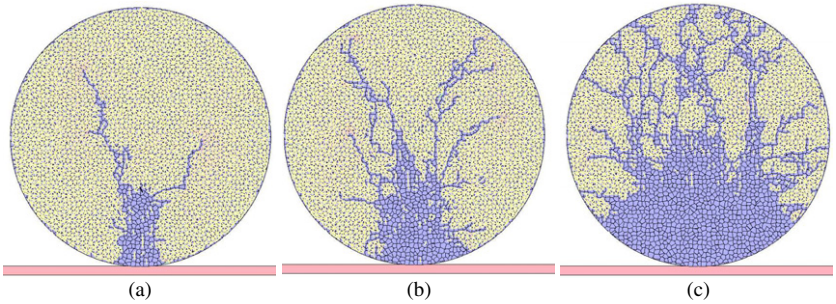

Figure 2. Final reassembled states of the break-up process of a disc of radius 30 cm at different impact velocities dropped on a hard frictionless plate. (a) $v_0 = 100$ cm s^{-1}. The cone is not fully developed and only a few oblique cracks are present. (b) $v_0 = 200$ cm s^{-1}. More oblique cracks develop and travel a greater distance. (c) $v_0 = 600$ cm s^{-1}. Both oblique cracks and secondary cracks are present.

reassembled into the initial disc. At low velocities the compressive wave intensity generated at the impact point is low, and hence the cone cannot develop fully. Moreover, only a few oblique cracks are obtained, and they do not reach the opposite surface of the disc (figure 2(a)). As the velocity increases, more oblique cracks develop and cover a greater distance (figure 2(b)) and a considerable part of the initial kinetic energy goes into the motion of the residue resulting in rebound. At the impact velocity where the oblique cracks reach the outer surface of the disc opposite to the impact point, the break-up process drastically changes: below this velocity mostly contact damage occurs in the form of the damage cone and a relatively big residue remains back. Above this velocity, however, the cracks spanning the entire disc result in the break-up of the residue into smaller pieces; see figure 1(d). Later on it will be shown that the behaviour of the system quantitatively changes at this velocity, which we call the critical velocity. At impact velocities larger than the critical value, secondary cracks are generated roughly perpendicular to the oblique cracks. Secondary cracks from neighbouring oblique cracks may merge with each other as can be seen in figure 2(c). Also at higher impact velocities, vertical cracks with a direction nearly perpendicular to the target plate are more prominent as the intensity of stress concentration near the tip region of the cone is high as compared to other parts.

Crack patterns obtained in the final state of oblique impacts at impact angles 75°, 60° and 45° are compared in figure 3. It is important to emphasize that in our calculations the friction between the target plate and the circular disc is completely excluded. Under this condition, varying the impact velocity while keeping its normal component constant, practically the same crack pattern is obtained (see figure 3). Thus, the crack propagation and orientation during the fragmentation process solely depend on the normal component of the impact velocity.

Comparing the crack pattern obtained in the simulations to the experimental results [1], we did not find any meridian cracks as they are difficult to detect in two dimensions. The pattern of oblique cracks and secondary cracks has a satisfactory agreement with the experimental results. The simulations confirm that oblique cracks which were observed in experimental investigations [1] develop along the trajectories of maximum compression planes.

4. Results

Studying the evolution of the final crack patterns when changing the impact velocity, we have identified a critical velocity v_c which separates the regimes of different break-up mechanisms.

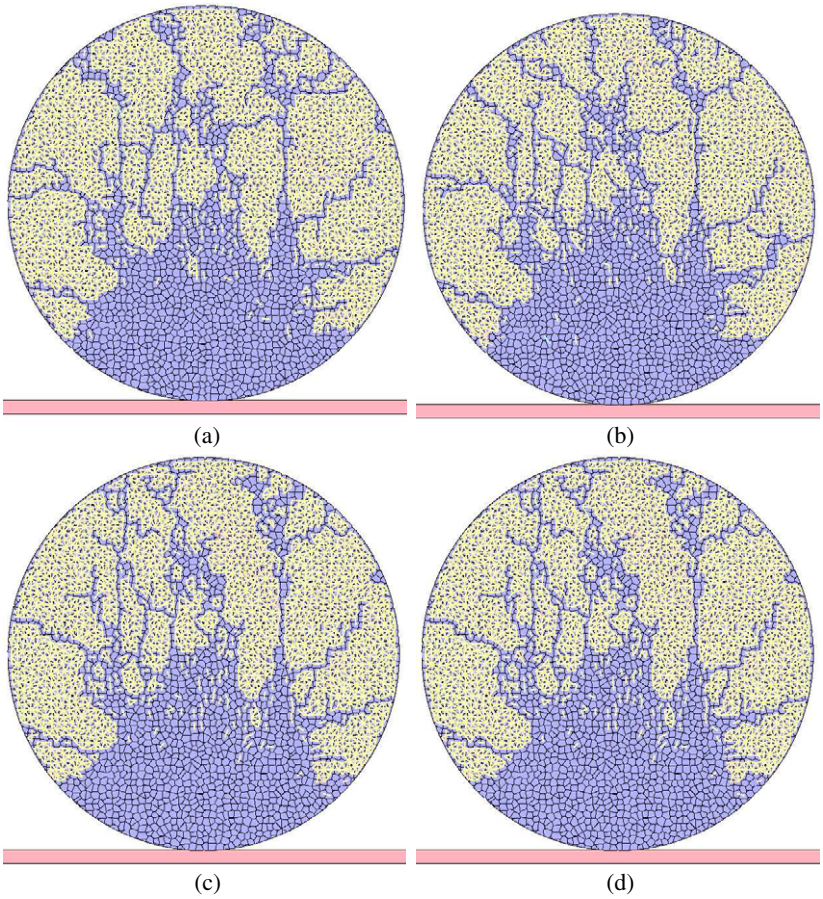

Figure 3. The reassembled snapshots of normal and oblique impacts at different velocities keeping the normal component constant as 500 cm s^{-1}. The crack patterns are almost the same in all cases. (a) $\theta = 90°$. (b) $\theta = 75°$. (c) $\theta = 60°$. (d) $\theta = 45°$.

In the following, we analyse characteristic quantities of the break-up process, and show that there are substantial differences between the two regimes.

4.1. Size distribution of fragments

Recently, it has been shown that the final outcome of a fragmentation process can be classified into two states depending on the amount of the imparted energy: damaged and fragmented states with a sharp transition in between. Detailed analysis revealed that the transition between the two states occurs as a continuous phase transition which also provides a possible explanation of the power law mass distribution of fragments observed [10].

To explore the nature of the critical velocity v_c identified in the previous section we investigated the evolution of the mass of the two largest fragments when varying the angle θ and the velocity v_0 of impact. Plotting the largest fragment mass as a function of the normal component of the impact velocity for both normal and oblique impacts in figure 4, all curves fall over one another. This implies that in the absence of friction between the plate and the disc the size reduction achieved depends both on v_0 and θ but in such a way that it depends on the combination of the two variables $v_n = v_0 \sin\theta$. The curves of the second largest mass

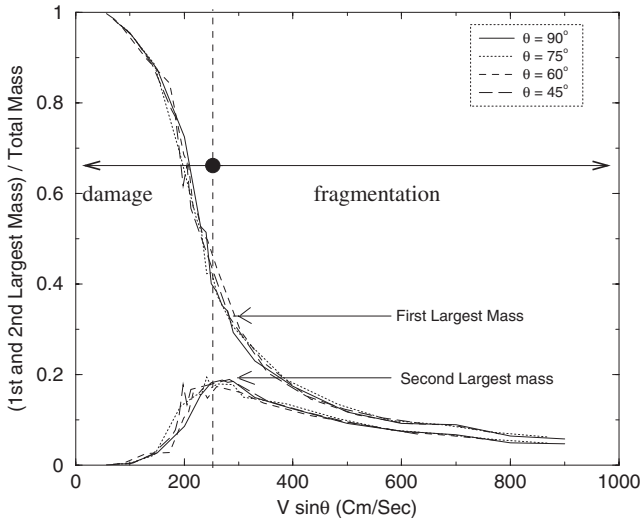

Figure 4. The mass of the first and second largest fragment as a function of the normal component of the impact velocity $v_0 \sin\theta$ at different impact angles θ and velocities v_0 for a system size 30 cm. The vertical dashed line indicates the critical point; furthermore, the damaged and fragmented regimes are also shown.

exhibit the same data collapse when plotting them as a function of v_n, further supporting the above arguments.

The functional form of the two largest fragment masses in figure 4 shows the existence of two distinct regions. At low impact velocity, breakage takes place only at the impact point and the largest fragment is nearly equal to the original mass. As the velocity of impact increases, more small fragments are chipped off from the impact point and cracks start around the damaged conical region and move towards the outer surface of the disc. At the critical velocity v_c these propagating cracks reach the outer surface opposite the impact point and the largest fragment breaks into several big pieces. The impact velocity where the second largest mass attains its maximum value or where there is an inflexion point in the largest fragment mass curve coincides with the critical velocity defined by analysing the cracking pattern in figures 1 and 2. In our case for normal impact of a system of 30 cm radius the critical velocity turned out to be 250 cm s^{-1}.

The quality of the data collapse of the curves in figure 4 obtained at different impact velocities v_0 and angles θ is excellent for the largest fragment; however, there are large fluctuations of the value of the second largest mass at impact velocities just below the critical point. Above the critical point all curves merge nicely together.

More information about the evolution of fragment sizes on varying impact angle θ and velocity v_0 can be obtained by studying the moments of fragment masses [10, 21, 26, 39]. The kth moment M_k of fragment masses is defined as

$$M_k = \sum_i^{N_f} m_i^k - M_{\max}^k, \tag{1}$$

where N denotes the total number of fragments, m_i is the mass of fragment i and $M_{\max}$ is the largest fragment mass. The definition equation (1) means that the kth power of the largest mass is extracted from the sum of the kth powers of the fragment masses. The average mass of fragments $\overline{M}$ can be defined as the ratio of the second and first moments $\overline{M} \equiv M_2/M_1$ [10].

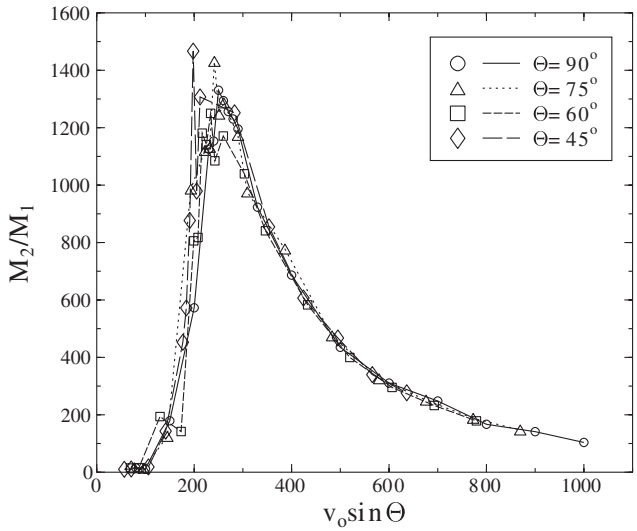

Figure 5. The average fragment mass $\overline{M} = M_2/M_1$ as a function of the normal component of the impact velocity v_0. For oblique impact when the velocity approaches the critical point fluctuations always arise; however, beyond the critical velocity all curves merge nicely.

In figure 5 the average fragment mass $\overline{M}$ is presented as a function of the normal component of the impact velocity v_0 for the system size $R = 30$ cm obtained at different impact angles θ. It can be seen that all the curves fall on top of each other, supporting again that the relevant variable of the system is $v_0 \sin\Theta$. Larger fluctuations arise below the critical point, which are more dominant for lower impact angles. Note that the position of the maximum in the inset coincides with the transition point determined in figure 4.

Studies of fragmentation of various types of brittle solids have revealed that a larger amount of energy is required to achieve the same size reduction on systems of larger size. However, in terms of the specific energy, i.e. the energy imparted to the fragmenting system divided by the total mass E_0/m_{tot}, all the characteristic quantities show a universal behaviour; in particular, the critical value of the specific energy is independent of the system size [10–12, 27, 38, 39]. For impacting discs, however, the critical value of the specific energy shows a clear dependence on the size of disc R as illustrated in figure 6. The larger the disc, the higher the energy density required to break it into pieces. A possible explanation is that for larger discs a larger part of the imparted energy goes into the motion of the fragments, lowering the efficiency of break-up.

The total number of fragments N_{f} is also an important measure of the degree of break-up in the impact process. Figure 7 shows that the number of fragments N_{f} is uniquely determined by the normal component of the impact velocity v_{n}; i.e., the curves obtained at different impact angles present a perfect collapse when plotting them as a function of v_{n}. It can be seen in the figure that the number of fragments is a monotonically increasing function of the velocity; however, the functional form of N_{f} seems to be different on the two sides of the critical point; i.e., up to the critical point the curves show clearly a straight line, whereas above the critical point all curves are slightly bent towards down as the efficiency of the fragmentation process decreases. Replotting the results using logarithmic scale on the horizontal axis, however, a straight line is obtained above the critical point (see the inset of figure 7), which implies that N_{f} has the form

$$N_{\mathrm{f}} = a \cdot \ln \frac{v_{\mathrm{n}}}{v_{\mathrm{nc}}} + N_{\mathrm{c}}, \qquad \text{for } v_{\mathrm{n}} > v_{\mathrm{nc}}, \tag{2}$$

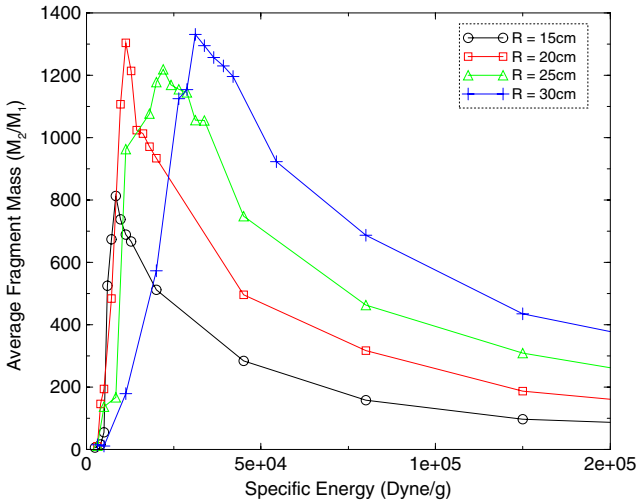

Figure 6. Average fragment mass $\overline{M} = M_2/M_1$ as a function of specific energy $E_0/m_{\rm tot}$. The critical point, i.e. the position of the maximum, depends on system size.

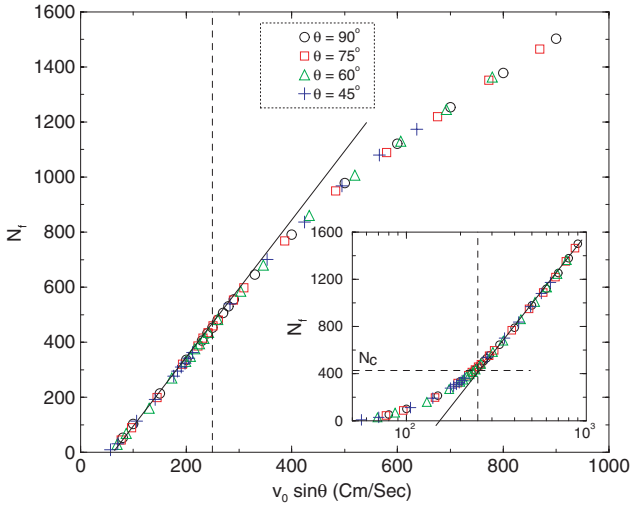

Figure 7. Number of fragments $N_{\rm f}$ as a function of the normal component of the impact velocity.

where $N_{\rm c}$ denotes the number of fragments at the critical point and a is the slope of the straight line in the inset of figure 7.

The amount of damage occurring during the break-up process can be quantified by the so-called damage ratio d proposed by Thornton *et al* [7]. d is defined as the ratio of the number of broken contacts $N_{\rm b}$ to the total number of contacts $N_{\rm c}$ existing initially inside the disc. The damage ratio d depends both on the impact angle θ and the impact velocity v_0, i.e., increasing v_0 at a fixed value of θ results in an increase of d; furthermore, increasing the impact angle θ at a given value of v_0, the damage ratio also increases. However, when plotting d as a function of the normal velocity $v_{\rm n}$ in figure 8 the curves obtained at different impact angles collapse on top of each other, which implies that d solely depends on $v_{\rm n}$. Similarly to the number of fragments, d is also a monotonically increasing function of $v_{\rm n}$; however, its functional form changes at

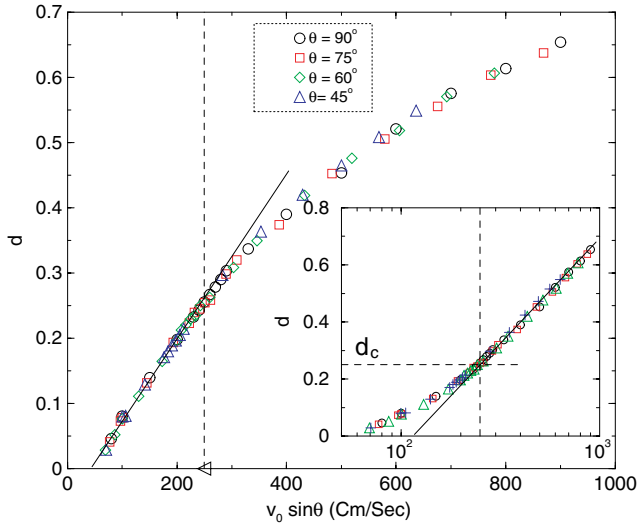

Figure 8. Dependence of damage ratio d, the number of broken beams N_b to the total number of beams N_o, on the normal component of the impact velocity.

the critical point. It is observed that below the critical point d is a linear function of v_n, while above the critical point the curve is non-linear, slightly bending down. On a semilogarithmic plot again a straight line arises, which implies the functional form

$$d = b \cdot \ln\left(\frac{v_n}{v_{cn}}\right) + d_c, \qquad \text{for } v_n > v_c \tag{3}$$

where d_c is the value of d at critical point and b is the slope of the fitted straight line in figure 8. A somewhat similar functional form of d has also been pointed out by Thornton [7, 31] in impact of discs and spherical objects with a hard plate.

4.2. Plate force

An alternative way of showing the effect of the impact angle is by analysing the force exerted by the plate on the disc. In figures 9(a) and (b) typical time series of the force between the target plate and the disc are presented. If the normal component of the impact velocity $v_n = v_0 \sin\theta$ is kept constant while changing θ and v_0, the force practically remains constant except for fluctuations; see figure 9(a). This shows clearly that the force exerted by the target plate only depends on the normal component of impact velocity, providing further support for the above findings in consistency with [7, 8, 31, 34].

To take a clear view of the nature of the plate force, we have plotted the plate force as a function of time at various velocities (see figure 9(b)). In general, as the impact velocity is increased, the maximum plate force increases and the duration of the impact decreases. The maximum force exerted by the plate occurs when the kinetic energy has a minimum (see figure 9(c)). The maximum plate force or minimum kinetic energy corresponds to the state of the fragmented disc where most of the bonds break near the contact region and cracks start to propagate radially outwards from the conical damage region (see figure 9(d)). Since damage, i.e. bond breaking, dissipates energy, the final kinetic energy is significantly less than the initial kinetic energy. Increasing the impact velocity gives rise to an increase in the final kinetic energy and decrease of the duration of plate–disc contact. Clearly, there are two stages

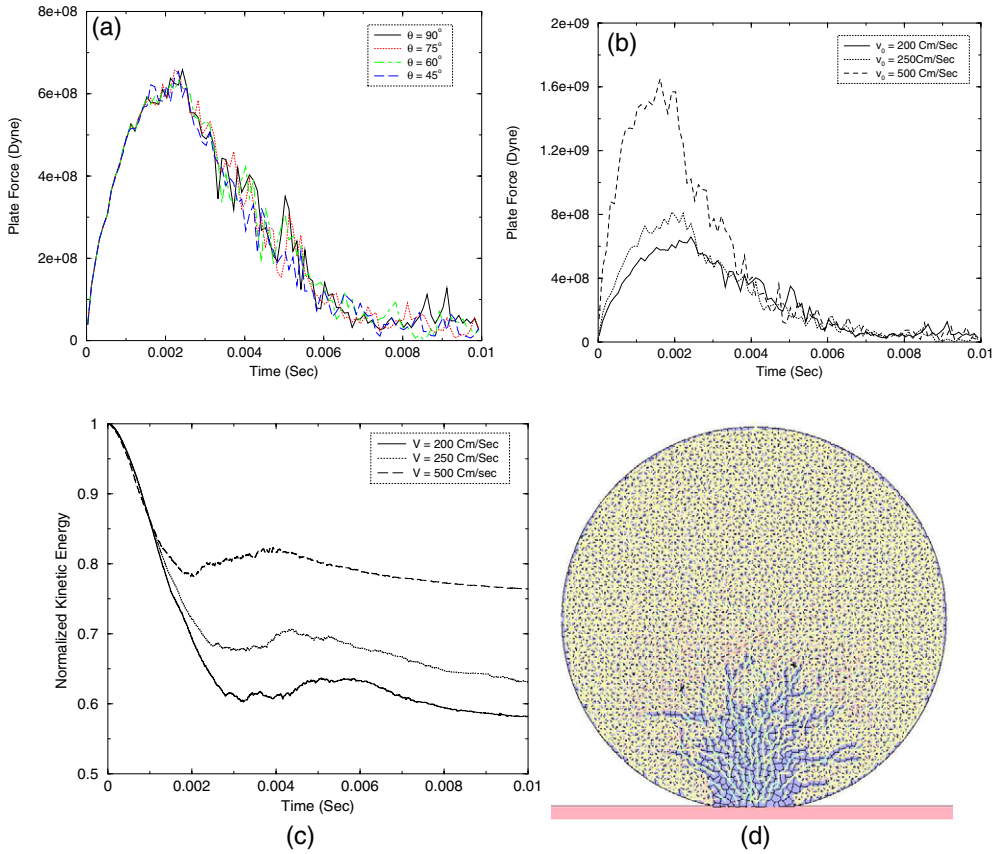

Figure 9. (a) Keeping the normal component of impact velocity constant at different impact angles, the force exerted by the plate is almost the same. (b) Force exerted by the plate at various velocities during normal impact. (c) The kinetic energy normalized by the total kinetic energy as a function of time. (d) The state of the disc of size 30 cm after $t = 0.002\,10$ s, which corresponds to the maximum plate force and minimum kinetic energy at the impact velocity of 250 cm s^{-1}.

to the bond breaking process during impact. Initially, bonds are broken primarily as a result of the high compressive shock wave adjacent to the impact site, which occurs during the period when the plate force is increasing. This is followed by further bond breakage due to crack propagation radially outwards, starting around the conical damage region where high stress concentration occurs, while the plate force decreases.

4.3. Mass distribution of fragments

The mass (or size) distribution of fragments is one of the most important characteristic quantities of the disc impact which has also a high practical relevance. The fragment mass histograms $F(m)$ of normal impact are presented in the figure 10, for the system size 30 cm at varying impact velocity v_0. In order to resolve the shape of the distribution over a wide range of mass values, logarithmic binning was used; i.e., the binning is equidistant on a logarithmic scale.

It can be observed that the histograms have a maximum at small fragment sizes due to the existence of single unbreakable polygons. The shape of the peak of the small fragments

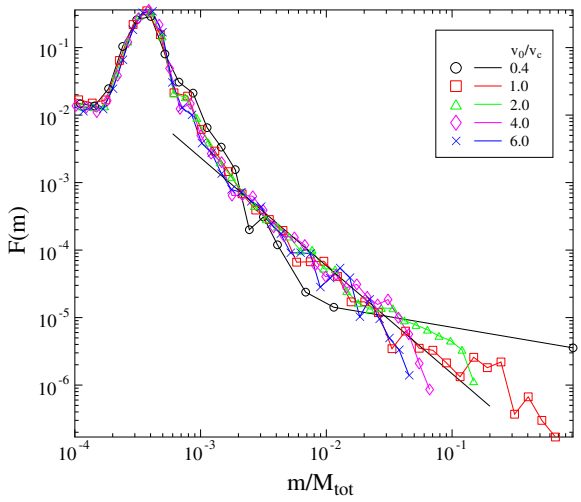

Figure 10. The fragment mass histograms of normal impact for the system size $R = 30$ cm at several initial impact velocities below and above the critical point v_c. The straight line shows the power law fit to the curve at the critical velocity $v_c = 250$ cm s^{-1} with an exponent $\tau = 1.8 \pm 0.08$.

is determined by the mass distribution of single Voronoi polygons obtained by the tessellation procedure. At low velocities, much below the critical point, the distributions are discontinuous: for small fragment masses the distributions are smoothly decreasing functions, while for large fragments $F(m)$ has a peak, indicating the presence of large unbroken pieces. In between, however, the medium sized fragments are missing. As the impact velocity increases, the large pieces break up into smaller ones, the peak of the large fragments on the right-hand side gradually disappears and the entire mass distribution becomes continuous. It is interesting to note that the peak of large fragments disappears completely at the critical point where the cracks starting from the damaged conical region reach the outer surface of the disc, breaking the disc into several smaller pieces. As a result, $F(m)$ takes a power law form at the critical point

$$F(m) \sim m^{-\tau}. \tag{4}$$

The exponent of the power law τ fitted to the curve at the critical velocity $v_0 = 250$ cm s^{-1} is $\tau = 1.8 \pm 0.08$. For oblique impact the value of the exponent is nearly the same as in normal impact within a precision of ± 0.05. Simulations with different system sizes such as $R = 25$, 20 and 15 cm proved that the exponent τ is also independent of R.

Increasing the impact velocity above the critical point, the power law regime of the mass distribution remains unchanged; however, the largest fragment size decreases and the shape of the curve attains an exponential form for large fragments. In the limiting case of very high impact velocities the disc suffers complete disintegration into small pieces. In this shattered phase $F(m)$ gradually transforms to an exponential form by decreasing the cut-off mass and shortening the power law regime. However, the shattered phase is slowly approached when increasing the impact velocity v_0 since the damage ratio and the number of fragments have a logarithmic dependence on v_0. The results are in good quantitative agreement with the experimental findings on the fragmentation of plate-like objects [14, 22, 29, 30].

4.4. Scaling of the velocity distribution

In applications like mineral processing, a fragment, formed with a certain velocity, can undergo secondary break-up due to collisions with other fragments or with the walls of the container.

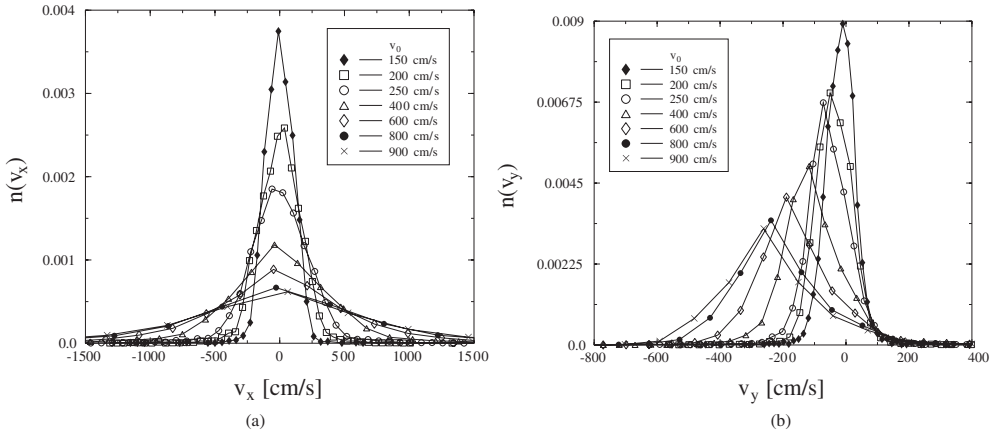

Figure 11. The distribution of the x and y components of the velocity of fragments with fixed system size $R = 30$ cm varying the initial impact velocity v_0.

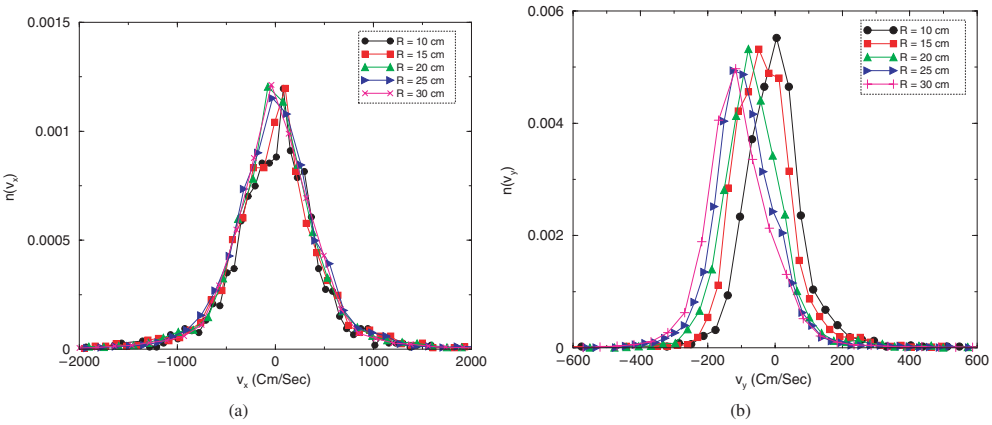

Figure 12. The distribution of the x and y components of the velocity of fragments with fixed impact velocity $v_0 = 400$ cm s^{-1} varying the radius R of the particle.

To get an estimate about the importance of this secondary fragmentation, it is essential to study the fragment velocities. We investigated the velocity distribution of fragments and its dependence on the macroscopic variables of the system like the impact velocity v_0 and radius of the disc R.

To determine the velocity distribution of fragments and explore its dependence on v_0 and R, we analysed the data in two ways. First we fixed the disc radius R and varied the impact velocity v_0, then fixed v_0 while varying R. In both cases the calculations are restricted to normal impact ($\theta = 90°$) and the distributions of the velocity components $n(v_x)$, $n(v_y)$ of the centre of mass of the fragments are evaluated. In figures 11 and 12 we present the results for fixed radius $R = 30$ varying the initial velocity and for fixed $v_0 = 400$ cm s^{-1} varying the radius of the particles, respectively. In figure 11(a) one can observe that the distribution of the x component of the fragment velocities $n(v_x)$ is symmetric about $v_x = 0$ as expected from the symmetry of the initial conditions. The zero mean value is a consequence of momentum conservation. As the impact velocity increases, the distribution broadens. The distribution $n(v_y)$ of the y

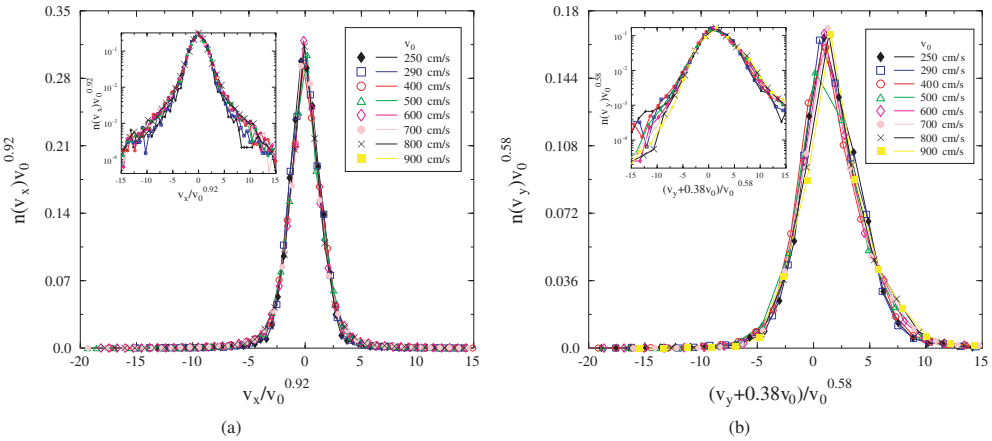

Figure 13. Rescaled plots of the velocity distributions for a fixed system size 30 cm varying the impact velocity v_0 above the critical point. The insets present the same curves on a lin–log plot.

components also broadens with increasing impact velocity but also shifts towards the negative y direction. This is obvious as the direction of the impact velocity is in the negative direction of the y axis and the total linear momentum increases with the impact velocity. However, in the y direction fragments are slower, i.e., the values of v_y are much smaller than those of v_x. Note that there is a small fraction of the debris which has velocity larger than v_0, in agreement with experimental findings [25]. When the impact velocity v_0 is fixed and the size of the disc R is varied, however, the distribution of the x components $n(v_x)$ remains the same (see figure 12(a)). For $n(v_y)$ a similar trend is observed as in the case of changing v_0, except that the distribution is less dispersed with varying R (figure 12(b)). To reveal the functional form of the dependence of $n(v_x)$ and $n(v_y)$ on the macroscopic variables v_0 and R we performed a scaling analysis of the distributions. Figures 13 and 14 demonstrate that by appropriate rescaling the axes one can merge the curves obtained at different values of the macroscopic variables onto a single curve. In the case of the x components, the transformation is a stretching and shrinking by a power of v_0 on the vertical and horizontal axis, respectively. However, for the y components, a combination of a linear shift and a shrinking by a power of v_0 is required. The good quality of the data collapse implies that the v_0 and R dependence of the distributions can be cast in the form

$$n(v_x, v_0) \sim v_0^{-\alpha} \phi\left(v_x v_0^{-\alpha}\right), \tag{5}$$

$$n(v_y, v_0) \sim v_0^{-\beta} \psi\left((v_y + \lambda_1 v_0) v_0^{-\beta}\right), \tag{6}$$

where the parameter values $\alpha = 0.92$, $\beta = 0.58$, and $\lambda_1 = 0.38$ were obtained by varying them until the best data collapse is obtained in figures 13 and 14. Similarly, at constant velocity while varying the system size R the functional form of the distribution $n(v_y)$ reads as

$$n(v_y, R) \sim R^{-\gamma} \xi\left((v_y + \lambda_2 R) R^{-\gamma}\right), \tag{7}$$

where $\gamma = 0.12$ and $\lambda_2 = 6.2$ provide the best collapse in figure 14. ϕ, ψ and ξ are scaling functions which seem to have a Gaussian-like shape in figures 13 and 14. The Gaussian shape of the scaling functions is further supported by the insets of figures 13 and 14, where the same curves are presented on a lin–log plot. The scaling forms equations (5)–(7) show that the widths of the scaling functions have a power law dependence on the impact velocity v_0 and on

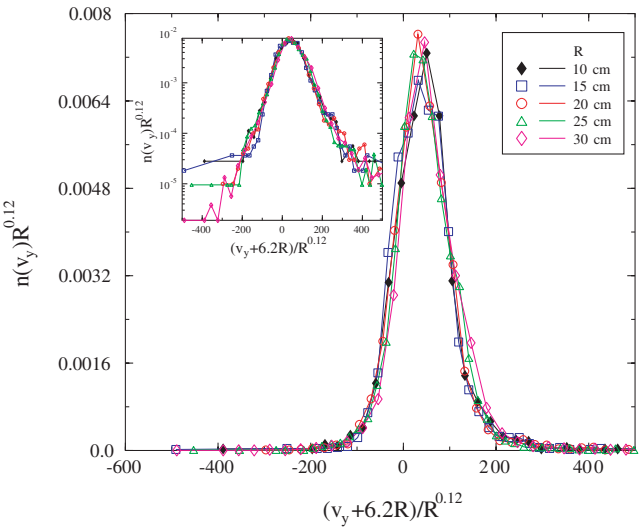

Figure 14. Rescaled plot of the distributions of the y component of fragment velocities $n(v_y)$ for a fixed impact velocity 400 cm s^{-1} varying the size R of the particle. The inset presents the same curves on a lin–log plot.

the radius of the disc R. It has to be emphasized that the above scaling behaviour is valid only above the critical velocity v_c; below v_c no scaling was found.

The scaling form of the distribution of the velocity components also has consequences for the spatial distribution of the flying pieces after impact. The increase of the width of the distributions with increasing impact velocity and disc radius implies that the flying fragments are more dispersed in space.

5. Conclusion

We studied the normal and oblique impact of a circular brittle particle on a hard frictionless plate using a cell model of cohesive granular materials. We carried out a detailed analysis of the evolution of the crack pattern arising in the disc during the impact process, and of the mass and velocity distributions of fragments in the final state.

For both normal and oblique impact, a cone shaped damage region is formed at the impact point whose base area increases gradually as the velocity of impact increases. Cracks start to develop from the conical damaged region where the maximum stress concentration exists. The oblique crack patterns obtained resemble those of the experimental findings [1], where oblique cracks moving along the plane of maximum compression were found. In agreement with the experimental observations, the oblique cracks in our simulation follow the trajectory of the maximum compression plane. Varying the impact velocities while keeping the normal component constant, we observed that the crack pattern remains the same in agreement with recent experimental and theoretical findings [1, 2, 4, 25, 33].

Our analysis showed the existence of a critical value of the impact velocity, at which the oblique cracks reach the outer surface of the disc opposite the impact point. The critical velocity separates two regimes of the break-up process; i.e. below the critical point only a damage cone is formed at the impact site (*damage*), cleaving of the particle occurs at the critical point, while above the critical velocity the disc breaks into several pieces (*fragmentation*). In the limit of very high impact velocities, the disc suffers complete disintegration into many small

fragments. However, this shattered phase is slowly approached since the damage ratio and the number of fragments increase logarithmically with the impact speed. The critical behaviour proved to be independent of the impact angle; it depends solely on the normal component of the impact velocity. Studying the average fragment size revealed that the critical value of the specific energy increases with the size of the disc. This implies in practical cases that a higher energy density is required to break a particle of larger size.

Above the critical point, the mass distribution $F(m)$ of fragments was found to obey the Gates–Gaudin–Schuhmann distribution (power law) with an exponent close to two. The power law functional form occurs at the critical point and remains unchanged in a broad interval of the impact velocity independent of the system size and of the impact angle. However, in the shattered phase attained in the limit of very high impact velocities the fragment mass distribution tends to an exponential form. The results are in good quantitative agreement with the experimental findings on the fragmentation of plate-like objects [14, 22, 29, 30].

In applications like mineral processing, a fragment, formed with a certain velocity, can undergo secondary break-up due to collisions with other fragments or with the walls of the container. To get an estimate about the importance of this secondary fragmentation, the study of fragment velocities is essential. We determined the distribution of the velocity components of fragments and analysed the scaling behaviour of the distributions when changing the macroscopic variables of the system, i.e. impact velocity v_0 and system size R. A very interesting anomalous scaling of the distribution functions was revealed with a power law dependence on v_0 and R.

In a variety of size reduction operations practiced by a wide range of industries, there is a particular interest in the net energy required to achieve a certain size reduction and the energy distribution of the fragments during the grinding process. To maximize the efficiency of such processes, it is important to know the breakage characteristics of the grinding materials. Our current work can provide some of this valuable information.

Acknowledgments

This work was supported by the Collaborative Research Center SFB381. FK acknowledges the financial support of research contracts NKFP-3A/043/04, OTKA M041537, T049209 and of the György Békési Foundation of the Hungarian Academy of Sciences.

References

[1] Arbiter N, Harris C C and Stamboltzis G A 1969 *Trans. Soc. Mining Eng. AIME* **119** 244
[2] Salman A D, Biggs C A, Fu J, Angyal I, Szabo M and Hounslow M Z 2002 *Powder Technol.* **128** 36
[3] Chau K T, Wu S Z, Zhu W C, Tang C A and Yu T X 2003 *Proc. 16th Conf. on ASCE Engineering Mechanics (University of Washington, Seattle, July 2003)*
[4] Salman A D and Gorham D A 1999 *Powder Technol.* **107** 179
[5] Data S and Mishra B K 1998 FFT analysis of charge dynamics in tumbling mill *M. Tech. Thesis*
[6] Turcotte D L 1986 *J. Geophys. Res.* **91 B2** 1921
[7] Thornton C, Yin K K and Adams M J 1996 *J. Phys. D: Appl. Phys.* **29** 424
[8] Mishra B K and Thornton C 2001 *Int. J. Miner. Process.* **61** 225
[9] Kun F and Herrmann H J 1996 *Comput. Meth. Appl. Mech. Eng.* **138** 3
[10] Kun F and Herrmann H J 1999 *Phys. Rev.* E **59** 2623
[11] Kun F and Herrmann H J 1996 *Int. J. Mod. Phys.* C **7** 837
[12] D'Addetta G A, Kun F, Ramm E and Herrmann H J 2001 From solids to granulates—Discrete element simulations of fracture and fragmentation processes in geomaterials *Continuous and Discontinuous Modelling of Cohesive-Frictional Materials* (*Springer Lecture Notes in Physics (LNP)* vol 568) (Berlin: Springer) pp 231–58

[13] Oddershede L, Dimon P and Bohr J 1993 *Phys. Rev. Lett.* **71** 3107
[14] Meibom A and Balslev I 1996 *Phys. Rev. Lett.* **76** 2492
[15] Ching E S C *et al* 1999 *Physica* A **265** 119
[16] Diehl A *et al* 2000 *Phys. Rev.* E **62** 4742
[17] Åström J, Kellomäki M and Timonen J 1997 *Phys. Rev.* E **55** 4757
[18] Ashurst W T and Holian B L 1999 *Phys. Rev.* E **59** 6742
[19] Inaoka H, Toyosawa E and Takayasu H 1997 *Phys. Rev. Lett.* **78** 3455
[20] Åström J and Timonen J 1997 *Phys. Rev. Lett.* **78** 3677
[21] Aström J A, Holian B L and Timonen J 2000 *Phys. Rev. Lett.* **84** 3061
[22] Arakawa M 1999 *Icarus* **142** 34
[23] Wittel F, Kun F, Herrmann H J and Kröplin B H 2004 *Phys. Rev. Lett.* **93** 035504
[24] Matsui T, Waza T, Kani K and Suzuki S 1982 *J. Geophys. Res.* **87 B13** 10968
[25] Fujiwara A and Tsukamoto A 1980 *Icarus* **142** 44
[26] Latora V, Belkacem M and Bonasera A 1994 *Phys. Rev. Lett.* **73** 1765
[27] Potapov A V, Campbell C S and Hopkins M A 1995 *Int. J. Mod. Phys.* C **6** 399
[28] Katsuragi H, Sugino D and Honjo H 2003 *Phys. Rev.* E **68** 046105
[29] Kadono T 1997 *Phys. Rev. Lett.* **78** 1444
[30] Kadono T and Arakawa M 2002 *Phys. Rev.* E **65** 035107(R)
[31] Kafui K D and Thornton C 1999 *Powder Technol.* **109** 113
[32] Tsoungui O, Vallet D, Charmet J-C and Roux S 1999 *Granular Matter* **2** 19
[33] Khanal M, Schubert W and Tomas J 2004 *Granular Matter* **5** 177
[34] Moreno R, Ghadiri M and Antony S J 2003 *Powder Technol.* **130** 132
[35] Kelly E G and Spottiswood D J 1982 *Introduction to Mineral Processing* (New York: Wiley)
[36] Moukarzel C and Herrmann H J 1992 *J. Stat. Phys.* **68** 911
[37] Tillemans H J and Herrmann H J 1995 *Physica* A **217** 261
[38] Potapov A V and Campbell C S 1998 *Fourth Year Progress Report* International Fine Particle Research Institute, Dept. of Mech. Eng., University of Southern California, USA
[39] Behera B, Kun F, MaNamara S and Herrmann H J 2004 *Preprint* cond-mat/0404057
[40] Buchholtz V, Freund J A and Poschel T 2000 *Eur. Phys. J.* B **16** 169
[41] Pöschel T 2000 *Dynamik Granularer Systeme: Theorie, Experimente und Numerische Experimente* (Berlin: Logos Verlag)